Role of wind-driven upwelling in the Atlantic Meridional Mode

Gregory R. Foltz[1] and Regina R. Rodrigues[2]

14 December 2011

[1]NOAA/Atlantic Oceanographic and Meteorological Laboratory, Miami, FL

[2]Department of Environmental Engineering, Federal University of Santa Catarina, Florianópolis, Brazil

Corresponding author: gregory.foltz@noaa.gov

Submitted to *Geophysical Research Letters*

Abstract

The role of wind-driven upwelling in the Atlantic Meridional Mode (AMM) is examined using observations and reanalysis products. It is found that upwelling plays an important role in the AMM through its influence on sea surface temperature (SST) in the equatorial North Atlantic (ENA: 2°N–8°N). During a positive phase of the AMM, anomalously weak upwelling and a deeper than normal thermocline in the ENA drive an anomalous increase in SST. Conversely, anomalously strong upwelling and a shallower than normal thermocline lead to anomalous cooling of SST in the ENA during negative AMM phases. The influence of wind-driven upwelling on the AMM is strongest during the seasonal peak of the AMM in boreal spring. This is the season when there is mean upwelling the ENA and the thermocline depth in the ENA is at its seasonal minimum. Evidence is found for positive feedback between anomalies of wind-driven upwelling in the ENA and the cross-equatorial gradient of SST. These results help to explain aspects of the AMM that cannot be explained solely by thermodynamic air-sea interactions.

1 Introduction

The Atlantic Meridional Mode (AMM) is the strongest source of coupled ocean - atmosphere variability in the tropical Atlantic on interannual to decadal timescales. It is characterized by an anomalous meridional gradient of sea surface temperature (SST) across the equator and a meridional displacement of the rain-producing intertropical convergence zone (ITCZ) [*Nobre and Shukla*, 1996; Fig. 1]. Rainfall in Northeast Brazil and tropical cyclone activity in the North Atlantic are influenced by the AMM through its control over the position of the ITCZ and atmospheric circulation in the tropical

North Atlantic [*Hastenrath and Greischar*, 1993; *Vimont and Kossin*, 2007].

The AMM is most pronounced during boreal spring, when SSTs in the equatorial Atlantic are warmest climatologically and the Atlantic ITCZ is most sensitive to changes in the cross-equatorial gradient of SST [*Chiang et al.*, 2002]. Positive wind-evaporation-SST (WES) feedback has been shown to contribute to the growth of the AMM and the southward propagation of SST and surface wind anomalies in the tropical North Atlantic [*Chang et al.*, 1997; *Xie*, 1999]. Recent studies suggest that oceanic mixed layer dynamics associated with wind-driven upwelling and equatorial waves govern SST variability in the tropical Atlantic equatorward of 15° [*Barreiro et al*, 2005; *Rodrigues et al.*, 2011; *Foltz et al.*, 2011]. However, these analyses were limited either to specific ENSO years [*Barreiro et al.*, 2005; *Rodrigues et al.*, 2011] or to a particular AMM event [*Foltz et al.*, 2011]. Here we investigate the contribution of wind-driven upwelling to the AMM during 1982–2010.

2 Data and methodology

Several satellite-based datasets and reanalysis products are used in this study. A combined satellite-in situ SST product is available weekly for the period 1981–2010 on a 1° grid [*Reynolds et al.*, 2002]. We use daily-averaged surface winds, specific humidity, air temperature, and shortwave radiation on a 2° grid from the NCEP/NCAR reanalysis, available during 1948–2010 [*Kalnay et al.*, 1996]. Monthly averages of NCEP/NCAR reanalysis wind speed, specific humidity, and air temperature, together with *Reynolds et al.* [2002] SST, are used in the *Fairall et al.* [2003] bulk flux algorithm to calculate the surface latent heat flux (LHF) during 1982–2010. Daily surface shortwave radiation (SWR) is available from a satellite-based dataset on a 2.5° grid for 1983–2008

[*Zhang et al.*, 2004]. These data are averaged to monthly means, and the time series is extended back to 1982 and forward through 2010 by adding NCEP/NCAR reanalysis SWR anomalies to the *Zhang et al.* [2004] monthly mean climatology.

Monthly averaged subsurface temperature and salinity are available during 1980–2010 on a $\frac{1}{3}^{\circ}$-lat$\times 1^{\circ}$-lon grid from the Global Ocean Data Assimilation System (GODAS) produced at NCEP [*Behringer and Xue*, 2004]. Mixed layer depth (MLD) is calculated from GODAS temperature and salinity using the criterion of a 0.07 kg m^{-3} increase in density from a depth of 5 m, following *de Boyer Montégut et al.* [2007]. We restrict our analysis to the 1982–2010 period, when all datasets are available.

The AMM here is defined as the first EOF of detrended SST averaged during March–May for 1982–2010, after removal of the monthly mean climatology at each grid point. The first EOF explains 59% of the SST variability, compared to 18% and 6% for the second and third EOFs, respectively. The spatial pattern of SST, winds, and rainfall associated with the AMM agrees well with that of *Nobre and Shukla* [1996], which is based on different datasets and an earlier time period (Fig. 1a).

A simplified mixed layer temperature balance equation is used to assess the importance of LHF, SWR, and wind-driven upwelling for generating SST anomalies associated with the AMM:

$$\frac{\partial SST}{\partial t} = \frac{LHF + SWR}{\rho c_p h} - H w_e \frac{\partial T}{\partial z} \tag{1}$$

Here h is the MLD, H is equal to zero when $w_e < 0$ and one when $w_e > 0$, w_e is wind-driven upwelling (positive upwards), calculated from NCEP/NCAR reanalysis winds using Ekman dynamics modified by linear friction and following *Foltz et al.* [2011], and $\partial T/\partial z$ is the vertical temperature gradient below the mixed layer (see Auxiliary

Text and Figs. S1–S3 for details of this calculation and a description of the associated uncertainties). Note that the upwelling term implicitly includes forcing from equatorial waves through their influence on $\partial T/\partial z$. We have neglected the longwave radiation (LWR), sensible heat flux (SHF), and horizonal advection terms in (1) since LWR and SHF are weak compared to SWR and LHF, and horizontal advection provides weak damping of $\partial SST/\partial t$ associated with the AMM [*Foltz and McPhaden*, 2006]. The LHF and SWR terms are defined as positive when they act to increase SST. After calculating each term in (1) we compute anomalies at each grid point during 1982–2010 by subtracting the corresponding monthly mean seasonal cycle.

3 Results

During 1982–2010 there are noticeable interannual variations of the AMM as well as longer timescale variability (Fig. 1b). The strongest SST signal associated with the AMM is located in the northeastern tropical Atlantic, with two bands of enhanced SST variability extending westward near 18°N and southwestward from 10°N at the African coast to 5°N at 40°W (Fig. 1a). Surface wind anomalies are strongest between 5°S–5°N and between 20°N–25°N. The equatorial wind anomalies are associated with a pronounced anomalous northward shift of the ITCZ.

In agreement with previous studies, it is found that interannual to decadal variability of SST in the tropical North Atlantic (TNA: 8°N–25°N) associated with the AMM is driven primarily by surface heat fluxes. There are significant contributions from LHF and SWR anomalies and from anomalies of mixed layer depth, through their influence on the volume of ocean over which the climatological surface heat flux is absorbed [Figs. 2a,b and Figs. S4–S7; *Carton et al.*, 1996; *Tanimoto and Xie*, 2002;

Foltz and McPhaden, 2006; *Doi et al.*, 2010]. Anomalous thinning of the mixed layer during positive phases of the AMM is strongest between 15°N and 25°N and is driven by a decrease in turbulent mixing associated with a decrease in surface wind speed and increase in surface heat flux (Fig. 2a,b and Figs. S4–S7). In the remainder of this section only conditions associated with the positive phase of the AMM are discussed. The opposite conditions apply to negative phases since the analysis is linear.

In the equatorial North Atlantic (ENA: 2°N–8°N) SST variability associated with the AMM is similar in magnitude to the variability in the TNA, and there is a similar reduction in surface wind speed (Figs. 1a, 2a). However, the anomalous warming in the ENA is less clearly linked to changes in the surface heat flux and mixed layer depth (Fig. 2a,b). There is weak warming from wind-induced LHF that is counteracted by strong cooling from a decrease in SWR due to the northward shift of the ITCZ. SST in the ENA is likely to have a strong influence on surface winds and convection, and hence the AMM, because of the close proximity of the ENA to the mean latitude of the ITCZ and the high mean SSTs in the ENA (27°C averaged during MAM in the ENA, comapared to 24°C in the TNA). We therefore analyze the causes of SST variability in the ENA.

During positive phases of the AMM, there is significant anomalous deepening of the thermocline in the ENA associated with anomalously weak upwelling and anomalous downwelling equatorial Rossby waves [Fig. 2c; *Foltz and McPhaden*, 2010]. The weaker than normal wind-driven upwelling is driven primarily by the meridional component of the surface wind stress through a mechanism similar to that proposed by *Chang and Philander* [1994] [Fig. 1a; *Foltz et al.*, 2011]. The combination of anomalously weak upwelling and a deeper than normal thermocline (and hence anomalously

weak $\partial T/\partial z$ below the mixed layer) in the ENA results in an anomalous warming tendency of SST from the vertical advection term in (1) (Fig. 2c).

In order to investigate the temporal evolution of the SST balance in the ENA region, we consider the terms in (1) averaged in the ENA and regressed onto the AMM time series in Fig. 1b. The regressions are performed from a lead of 4 months (corresponding to the Dec before the Apr peak of the AMM) to a lag of one month (corresponding to the May following the Apr peak) (Fig. 3). SST in the ENA increases anomalously by about 0.1°C per month between Dec and Apr leading up to a positive AMM event (Fig. 3a). Anomalous warming from LHF is strongest during Jan, when surface winds are anomalously weak (Fig. 3b). During Feb–May there is weak and statistically insignificant warming from LHF despite a significant reduction in wind speed. The weaker LHF-induced warming is due to negative feedback from the anomalous air-sea humidity difference, tending to cool SST anomalously. The SWR term acts to cool SST anomalously in the ENA during Apr, when the northward anomalous shift of the ITCZ is most pronounced (Figs. 1a, 3b). As a result, the combination of anomalies in LHF and SWR tends to cool SST by 0.2°C during Dec–May, whereas observed SST increases by 0.3°C (Fig. 3a,b). In contrast, the sum of LHF and SWR in the TNA region explains the anomalous increase in SST there to within 0.1°C (Fig. 2 and Fig. S5).

The main cause of the anomalous increase in SST in the ENA during positive AMM events is a reduction in cooling from vertical temperature advection. Vertical advection tends to increase SST anomalously by 0.7±0.4°C during Dec–May, in agreement with the sum of the observed anomalous warming of 0.3°C and anomalous cooling of 0.2°C from the surface heat flux. The strongest anomalous warming from vertical

advection occurs during MAM, when there is climatological upwelling in the ENA and when anomalies of wind-driven upwelling therefore contribute to vertical temperature advection through (1) (Fig. 3c and Fig. S1). Boreal spring is also the season when the thermocline is shallowest climatologically and SST is therefore most sensitive to anomalies in upwelling and thermocline depth [e.g., *Foltz et al.*, 2011]. Results are similar for different ocean reanalysis products (Figs. S8, S9).

The importance of vertical advection in the SST balance of the ENA region, combined with the efficiency with which meridional SST gradients drive surface winds in the equatorial Atlantic [*Chiang et al.*, 2001], suggests that there may be a positive feedback between the cross-equatorial SST gradient (CESG), surface winds, and vertical temperature advection. If such a feedback were active, there should be significant positive lead/lag correlations between the CESG and vertical temperature advection. We would also expect the correlations to be nearly symmetric with respect to zero lag, an indication that vertical advection drives variability of the CESG and vice versa. A similar lagged correlation relationship would be expected between thermocline depth and CESG since changes in thermocline depth, driven by wind-driven upwelling and equatorial Rossby waves, affect vertical temperature advection through their influence on $\partial T/\partial z$.

Consistent with a possible positive wind-vertical advection-SST feedback, the correlations between the CESG and vertical temperature advection and between the CESG and thermocline depth are both positive and significant at leads/lags of zero to three months (Fig. 4b). The correlations between CESG and thermocline depth are highly symmetric about zero lag, whereas the correlations between CESG and vertical advection are slightly higher when CESG leads (Fig. 4b). In contrast, the

lead/lag correlation plots of the CESG with wind speed and LHF peak when SST lags, and compared to the correlations with vertical advection and thermocline depth, the strengths of the wind and LHF correlations drop more rapidly when SST leads (Fig. 4a). It is therefore possible that positive wind-vertical advection-SST feedback is active in the equatorial Atlatnic during AMM events and acts to sustain the AMM against damping. It appears that WES feedback is weaker and that wind-induced evaporation is driving a portion of the SST variability in the ENA, but not responding strongly to the CESG.

4 Summary and discussion

Mechanisms driving SST variability associated with the Atlantic Meridional Mode were investigated for the period 1982–2010. In agreement with previous studies, it was found that the surface heat flux drives most of the SST variability in the tropical North Atlantic (8°N–25°N). In the equatorial North Atlantic (2°N–8°N) anomalous wind-driven convergence and deepening of the thermocline drive anomalous warming of SST during positive AMM events, and conversely anomalous wind-driven divergence and shoaling of the thermocline force anomalous cooling during negative AMM events. Statistical analysis suggests a positive feedback between the cross-equatorial gradient of SST, surface equatorial winds, and vertical temperature advection may be active in the equatorial North Atlantic during boreal spring. These results therefore offer explanations for two aspects of the AMM that simple thermodynamically coupled models cannot fully explain: The strong SST signal in the eastern equatorial North Atlantic where wind-evaporation-SST feedback is weak [e.g., *Chang et al.*, 2001], and the timing of the peak of the AMM in boreal spring, when the thermocline is shallowest

climatologically in the equatorial North Atlantic. Experiments with coupled models will be helpful for quantifying the contributions of wind-evaporation-SST feedback and wind-vertical advection-SST feedback to the AMM.

References

Barreiro, M., P. Chang, L. Ji, R. Saravanan, and A. Giannini (2005), Dynamical elements of predicting boreal spring tropical Atlantic sea-surface temperatures, *Dyn. Atmos. Oceans*, *39*, 61–85, doi:10.1016/j.dynatmoce.2004.10.013.

Behringer, D. W., and Y. Xue (2004), Evaluation of the Global Ocean Data Assimilation System at NCEP: The Pacific Ocean. Preprints, *Eighth Symp. on Integrated Observing and Assimilation Systems for Atmosphere, Oceans, and Land Surface*, Seattle, WA, Amer. Meteor. Soc., 2.3.

Carton, J. A., X. H. Cao, B. S. Giese, and A. M. daSilva (1996), Decadal and interannual SST variability in the tropical Atlantic Ocean, *J. Phys. Oceanogr.*, *26*, 1165–1175.

Chang, P., and S. G. Philander (1994), A coupled ocean-atmosphere instability of relevance to the seasonal cycle, *J. Atmos. Sci.*, *51*, 3627–3648.

Chang, P., L. Ji, and H. Li (1997), A decadal climate variation in the tropical Atlantic Ocean from thermodynamic air-sea interactions, *Nature*, *385*, 516–518.

Chang, P., L. Ji, and R. Saravanan (2001), A hybrid coupled model study of tropical Atlantic variability, *J. Climate*, *14*, 361–390.

Chiang, J. C. H., S. E. Zebiak, and M. A. Cane (2001), Relative roles of elevated heating and surface temperature gradients in driving anomalous surface winds over tropical oceans, *J. Atmos. Sci.*, *58*, 1371–1394.

Chiang, J. C. H., Y. Kushnir, and A. Giannini (2002), Deconstructing Atlantic Intertropical Convergence Zone variability: Influence of the local cross-equatorial sea surface temperature gradient and remote forcing from the eastern equatorial Pacific, *J. Geophys. Res.*, *107*, 4004, 10.1029/2000JD000307.

de Boyer Montégut, C., J. Mignot, A. Lazar, and S. Cravatte (2007), Control of salinity on the mixed layer depth in the world ocean: 1. General description, *J. Geophys. Res.*, *112*, C06011, doi:2006JC003953.

Doi, T., T. Tozuka, and T. Yamagata (2010), The Atlantic meridional mode and its coupled variability with the Guinea Dome, *J. Climate*, *23*, 455–475.

Fairall, C. W., E. F. Bradley, J. E. Hare, A. A. Grachev, and J. B. Edson (2003), Bulk parameterization of air-sea fluxes: Updates and verification for the COARE algorithm, *J. Climate*, *16*, 571–591.

Foltz, G. R., and M. J. McPhaden (2006), The role of oceanic heat advection in the evolution of tropical North and South Atlantic SST anomalies, *J. Climate*, *19*, 6122–6138.

Foltz, G.R., and M.J. McPhaden (2010), Interaction between the Atlantic meridional and Niño modes, *Geophys. Res. Lett.*, *37*, L18604, doi:10.1029/2010GL044001.

Foltz, G. R., M. J. McPhaden, and R. Lumpkin (2011), A strong Atlantic Meridional Mode event in 2009: The role of mixed layer dynamics, *J. Climate*, doi: 10.1175/JCLI-D-11-00150.1, in press.

Hastenrath, S., and L. Greischar (1993), Circulation mechanisms related to Northeast Brazil rainfall anomalies, *J. Geophys. Res.*, *98*, 5093–5102.

Kalnay, E., et al. (1996), The NCEP/NCAR 40-year reanalysis project, *Bull. Amer. Meteor. Soc.*, *77*, 437–471.

Nobre, C., and J. Shukla (1996), Variation of sea surface temperature, wind stress, and rainfall over the tropical Atlantic and South America, *J. Climate*, *9*, 2464–2479.

Reynolds, R. W., N. A. Rayner, T. M. Smith, D. C. Stokes, and W. Q. Wang (2002), An improved in situ and satellite SST analysis for climate, *J. Climate*, *15*, 1609–1625.

Rodrigues, R. R., R. J. Haarsma, E. J. D. Campos, and T. Ambrizzi (2011), The impacts of inter-El Niño variability on the tropical Atlantic and Northeast Brazil climate, *J. Climate*, *24*, 3402–3422.

Tanimoto, Y., and S. P. Xie (2002), Inter-hemispheric decadal variations in SST, surface wind, heat flux, and cloud cover over the Atlantic Ocean, *J. Meteor. Soc. Japan*, *80*, 1199–1219.

Vimont, D. J., and J. P. Kossin (2007), The Atlantic Meridional Mode and hurricane activity, *Geophys. Res. Lett.*, *34*, L07709, doi:10.1029/2007GL029683.

Xie, S. P. (1999), A dynamic ocean-atmosphere model of the tropical Atlantic decadal variability, *J. Clim.*, *12*, 64–70.

Zhang, Y., W. B. Rossow, A. A. Lacis, V. Oinas, and M. I. Mishchenko (2004), Calculation of radiative fluxes from the surface to top of atmosphere based on ISCCP and other global data sets: Refinements of the radiative transfer model and the input data, *J. Geophys. Res.*, *109*, D19105, doi:10.1029/2003JD004457.

255

256

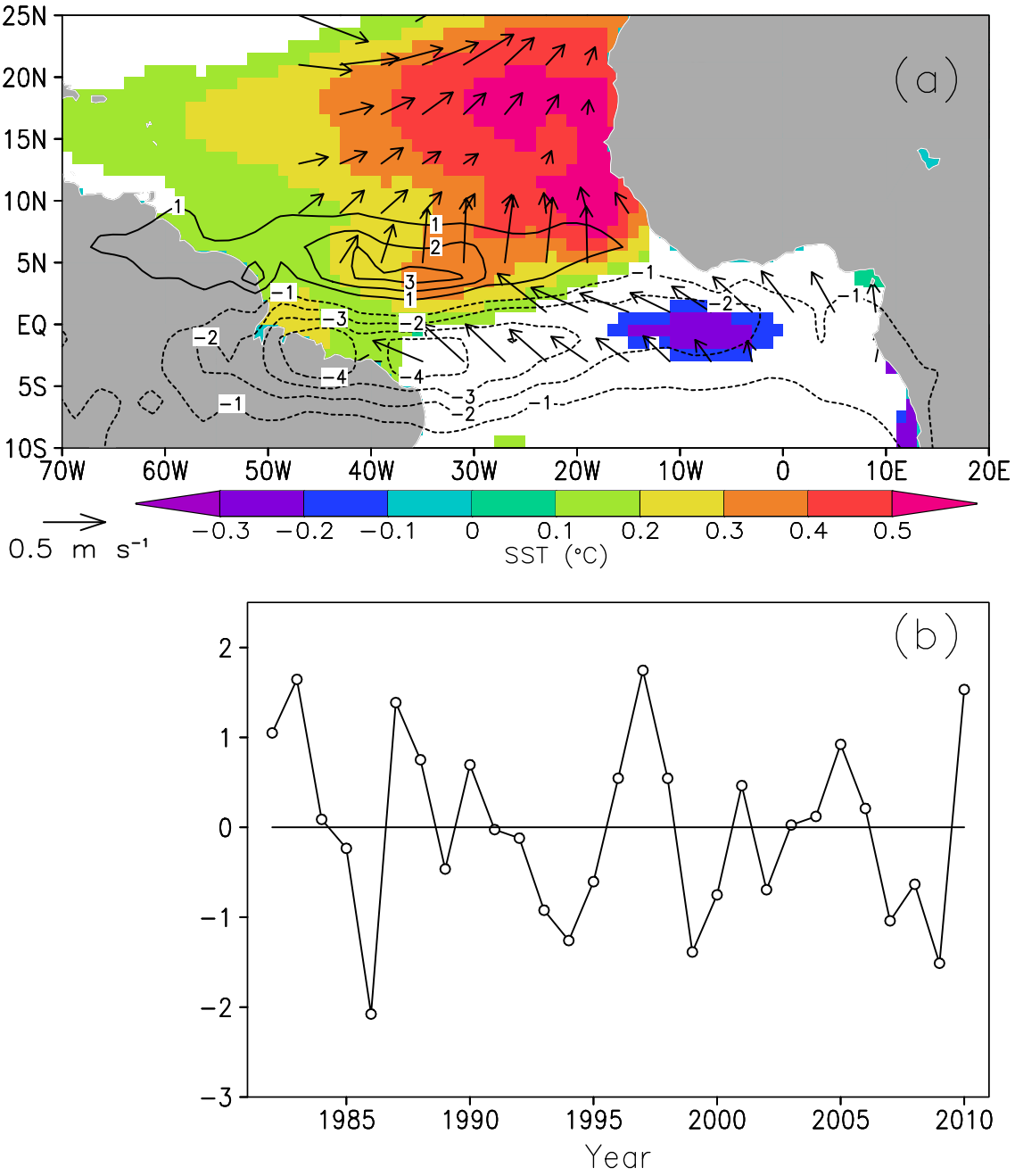

Fig. 1 (a) First EOF of MAM SST during 1982-2010 (shaded). The monthly mean seasonal cycle was removed before computing the EOF. Contours are GPCP rainfall (cm mo^{-1}) regressed onto the EOF time series, vectors are NCEP reanalysis surface winds. SST and rainfall are plotted only where significant at the 95% level. Wind vectors are plotted only where wind speed is significant at 95%. (b) Time series of the first EOF of MAM SST.

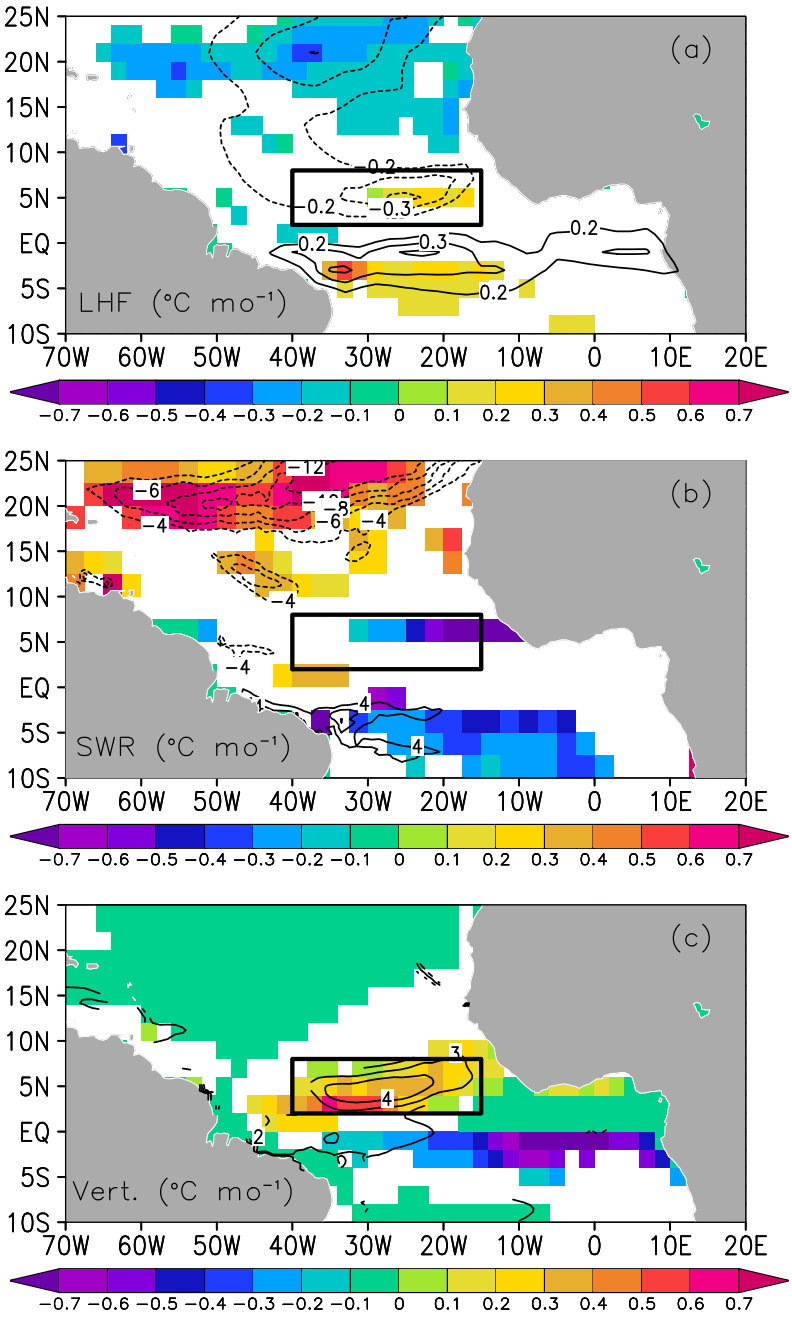

Fig. 2 (a) MAM wind speed (contours, m s^{-1}) and latent heat flux (shaded, °C mo^{-1}, positive indicates warming of the ocean) anomalies regressed onto the first EOF of MAM SST (shown in Fig. 1). Values are shown only where significant at the 95% level. (b) Same as (a) except anomalies of mixed layer depth (contours, m) and surface shortwave radiation (shaded, °C mo^{-1}). (c) Same as (a) except contours are thermocline depth (estimated as the depth of the 20°C isotherm in meters) and shading is vertical temperature advection at the base of the mixed layer (°C mo^{-1}). Boxes enclose the equatorial North Atlantic (ENA) region.

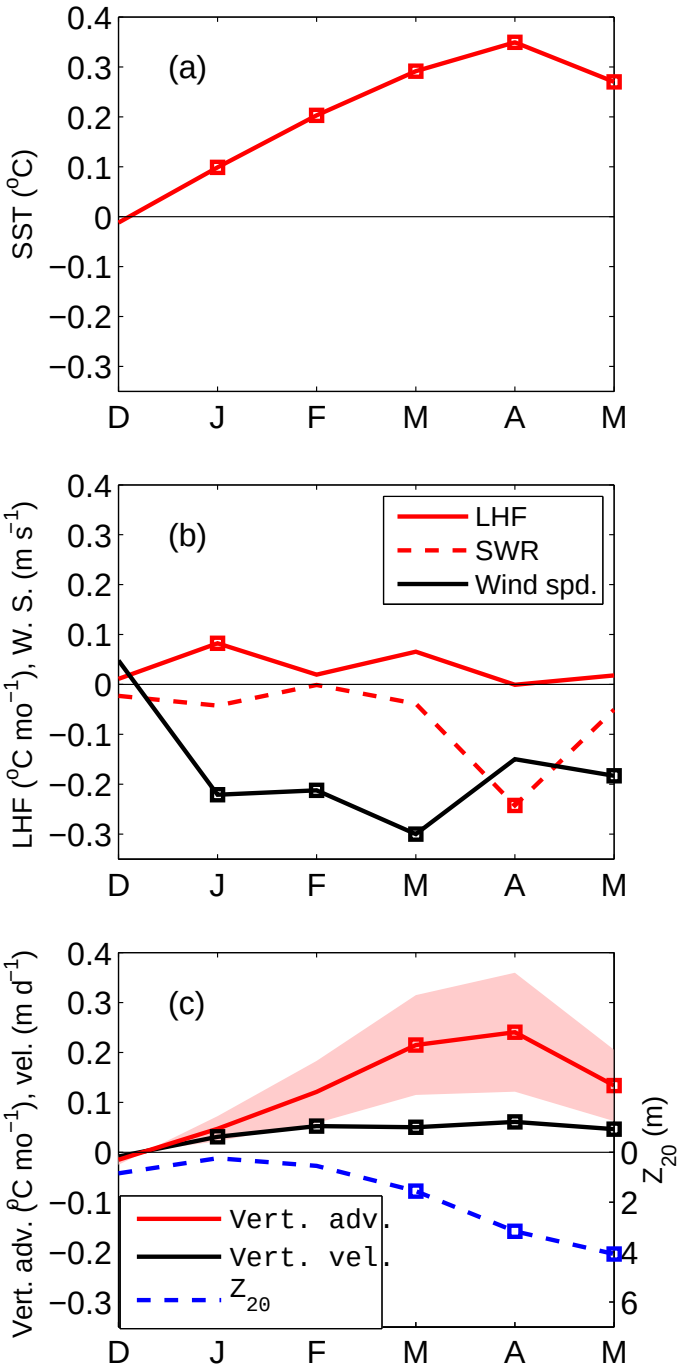

Fig. 3 (a) SST averaged in the ENA region (2°N–8°N, 15°W–40°W) and regressed onto the first EOF of MAM SST during Dec–May 1982–2010. Squares indicate regression coefficients that are significant at the 95% level. (b) Same as (a) except for latent heat flux (solid red), surface shortwave radiation (dashed red), and surface wind speed (black). (c) Same as (a) except for vertical advection at the base of the mixed layer (red, shading represents uncertainty estimates) and wind-driven upwelling (black, positive downward), and depth of the 20°C isotherm (dashed blue). Squares indicate values that are significant at the 95% level. Positive values of LHF, SWR, and vertical advection (red curves in (b) and (c)) indicate warming of SST.

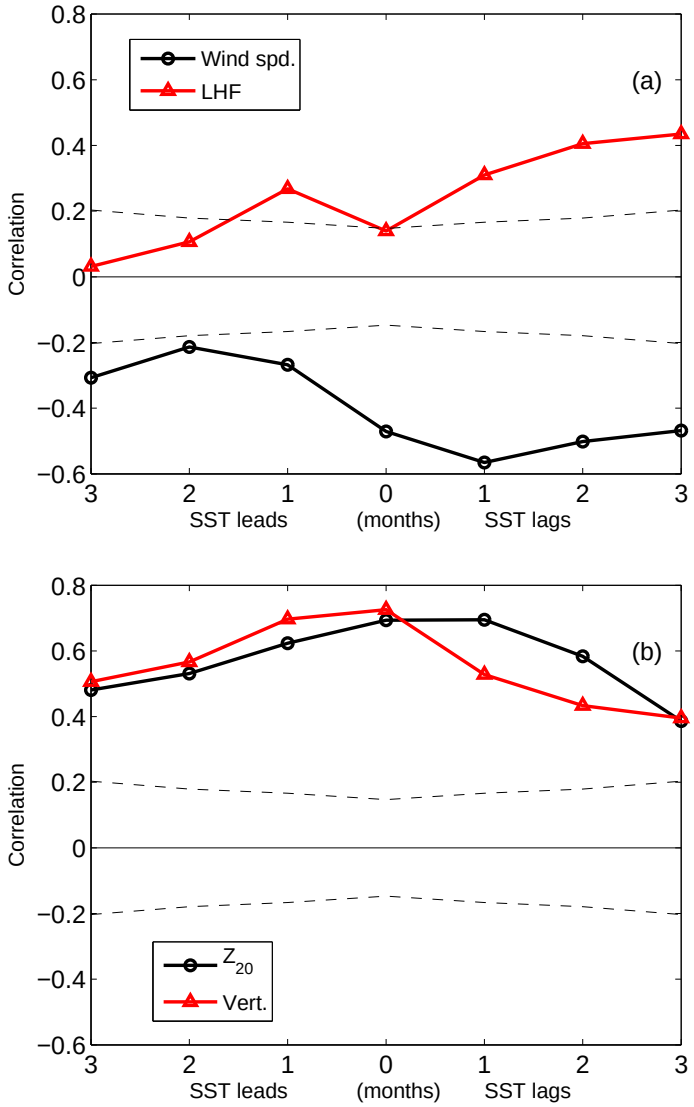

Fig. 4 (a) Lagged correlations of wind speed (solid black) and latent heat flux (red), averaged in the ENA region (2°N–8°N, 15°W–40°W), with the cross-equatorial gradient of SST, defined as SST in the ENA minus SST averaged between 0°–8°S, 0°–30°W. Correlations are performed for 1982–2010 during Jan–Jun. (b) Same as (a) except for depth of the 20°C isotherm (black) and vertical advection (red). Dashed lines are the 95% significance level.

Auxiliary Material

In this supplement we first present the details of the vertical temperature advection calculation. We then describe the SST balance in the tropical North Atlantic in more detail than was presented in the main text and compare the results using GODAS mixed layer depth, thermocline depth, and $\partial T/\partial z$ to those using SODA [*Carton et al.*, 2000].

Vertical temperature advection

Vertical temperature advection at the base of the mixed layer (last term in the right in (1)) depends on the rate of wind-driven upwelling and the vertical temperature gradient. Ideally both of these quantities would be calculated at the base of the mixed layer. In reality, it is difficult to calculate the depth-dependence of wind-driven currents, so we rely on a bulk model that gives horizontal currents averaged in the upper 30 m [*Lagerloef et al.*, 1999; *Foltz et al.*, 2011]. The 30 m depth scale is close to the average mixed layer depth of 33 m averaged in the equatorial North Atlantic during MAM.

To calculate $\partial T/\partial z$ in (1), we assume that water upwelled into the mixed layer originated from a depth of 15 m below the base of the mixed layer. This value is in the middle of the range used in previous studies [*McPhaden*, 1982; *Hayes et al.*, 1991; *Wang and McPhaden*, 1999; *Foltz et al.*, 2010, 2011]. The vertical temperature gradient is then calculated between the base of the mixed layer and 15 m below the base of the mixed layer. Using a value of 15 m assumes that turbulent mixing extends 15 m below the base of the mixed layer, and that water entrained into the 15-m layer below the mixed layer is eventually incorporated into the mixed layer. The extension of turbulent mixing below the base of the mixed layer is a consequence of our choice

of a mixed layer depth criterion that is based on density instead of vertical mixing rate. Lower and upper bounds on vertical temperature advection are calculated using depths of 10 m and 20 m below the mixed layer, respectively, for the calculation of $\partial T/\partial z$. These bounds are shown as error bars in Fig. 3c.

Vertical advection in (1) affects SST only when there is wind-driven divergence and upwelling ($w_e > 0$). This criterion is met during MAM throughout most of the equatorial North Atlantic (Fig. S1). Anomalies of w_e and $\partial T/\partial z$ in this region therefore have the potential to exert a significant impact on SST and the AMM.

An alternative method of calculating the vertical heat flux at the base of the mixed layer is to assume that it is accomplished entirely through vertical turbulent diffusion, which can be parameterized in terms of a constant diffusivity coefficient, K_v [e.g., *Hayes et al.*, 1991; *Wang and McPhaden*, 1999; *Foltz et al.*, 2011]:

$$\left(\frac{\partial SST}{\partial t}\right)_{vert} = -\frac{K_v}{h}\frac{\partial T}{\partial z} \tag{2}$$

Here h is the mixed layer depth and $\partial T/\partial z$ is the temperature gradient between the base of the mixed layer and 15 m below the base of the mixed layer. We use a value of $K_v = 1 \times 10^{-4}$ m^2 s^{-1}, which is in the lower end of the range found by *Hayes* et al. [1991] and *Wang and McPhaden* [1999] in the Pacific. An upper bound on vertical turbulent diffusion is estimated using $K_v = 1.5 \times 10^{-4}$ m^2 and calculating $\partial T/\partial z$ between the base of the mixed layer 20 m below the mixed layer. A lower bound is calculated using $K_v = 0.5 \times 10^{-4}$ m^2 and calculating $\partial T/\partial z$ between the base of the mixed layer 10 m below the mixed layer. The amplitude of the vertical diffusion term (2) is similar to that of the vertical advection term (1) (Fig. S2). Both terms are strongest during MAM and reach statistical significance during these months. The lead/lag correlations

with the cross-equatorial gradient of SST are also similar for advection and diffusion (Fig. S3).

SST balance

Here we expand on the SST budget analysis presented in the main text by first showing the terms in (1) in the tropical Atlantic during DJF (Fig. S4) and averaged in the tropical North Atlantic (TNA: 8°N–20°N, 20°W–45°W) during Dec–May (Fig. S5). We then discuss the contribution of the latent and shortwave heat fluxes (first two terms on the left in (1)) to anomalous changes in SST (in °C mo^{-1}) in comparison to the latent and shortwave fluxes (in W m^{-2}) in order to show the role of anomalies in mixed layer depth (Figs. S6, S7). Finally, we test the sensitivity of the SST balance results to the choice of reanalysis products by showing results based on SODA mixed layer depth and $\partial T/\partial z$ (Figs. S8, S9).

During the three months prior to the peak of a positive AMM event (DJF), there is a significant decrease in wind speed and a slight thinning of the mixed layer between 8°N–25°N (Fig. S4a,b). The competing SST tendencies from changes in wind-induced LHF and mixed layer depth result in an insignificant contribution from the latent heat flux to anomalous changes in SST. In contrast, the anomalous thinning of the mixed layer causes significant positive anomalies of shortwave radiation (Fig. S4b). There is weak anomalous cooling from vertical advection during DJF in a large portion of the tropical North Atlantic, but insignificant changes in vertical advection in the equatorial North Atlantic (2°N–8°N).

The SST balance averaged in the TNA shows a significant anomalous increase in SST during Jan–May that is driven by significant positive anomalies of the shortwave

radiation term, tending to increase SST, partially balanced by negative anomalies of latent heat flux (Fig. S5). Positive anomalies of the shortwave term are driven primarily by the anomalous thinning of the mixed layer as opposed to changes in the surface shortwave radiation (Figs. S6, S7). Negative anomalies of the latent heat flux term are also caused mainly by anomalous thinning of the mixed layer. In contrast, in the equatorial North Atlantic the contributions of shortwave and latent heat fluxes to SST are mainly through changes in the surface fluxes themselves and not changes in mixed layer depth (Figs. S6, S7).

In order to test the sensitivity of our results to the choice of ocean reanalysis products, we have recalculated the SST budget analysis using SODA and NCEP/NCAR reanalysis. The results are similar to those using GODAS and NCEP/NCAR (Figs. S8, S9). Anomalies of latent, shortwave, and vertical advection are weak during DJF (Fig. S8). There is significant cooling from the latent heat flux and warming from shortwave during MAM that is driven mainly by anomalous thinning of the mixed layer (Fig. S9a,b). There is also significant warming from the vertical advection term in the equatorial North Atlantic during MAM and cooling along and south of the equator, in agreement with the results based on GODAS (Fig. S9c).

References

Carton, J. A., X. Cao, G. Chepurin, and B. S. Giese (2000), A Simple Ocean Data Assimilation retrospective analysis of the global ocean 1950–1995, *J. Phys. Oceanogr.*, *30*, 294–309.

Foltz, G. R., J. Vialard, B. P. Kumar, and M. J. McPhaden (2010), Seasonal mixed layer heat balance of the southwestern tropical Indian Ocean, *J. Climate*, *23*,

947–965.

Foltz, G. R., M. J. McPhaden, and R. Lumpkin (2011), A strong Atlantic Meridional Mode event in 2009: The role of mixed layer dynamics, *J. Climate*, doi: 10.1175/JCLI-D-11-00150.1, in press.

Hayes, S. P., P. Chang, and M. J. McPhaden (1991), Variability of the sea surface temperature in the eastern equatorial Pacific during 1986–88, *J. Geophys. Res.*, *96*, 10553–10566.

Lagerloef, G. S. E., G. T. Mitchum, R. B. Lukas, and P. P. Niiler (1999), Tropical Pacific near-surface currents estimated from altimeter, wind, and drifter data, *J. Geophys. Res.*, *104*, 23313–23326.

McPhaden, M. J. (1982), Variability in the central equatorial Indian Ocean, Part II: Oceanic heat and turbulent energy balances, *J. Marine Res.*, *40*, 403–419.

Wang, W. M., and M. J. McPhaden (1999), The surface-layer heat balance in the equatorial Pacific Ocean. Part I: Mean seasonal cycle, *J. Phys. Oceanogr.*, *29*, 1812–1831.

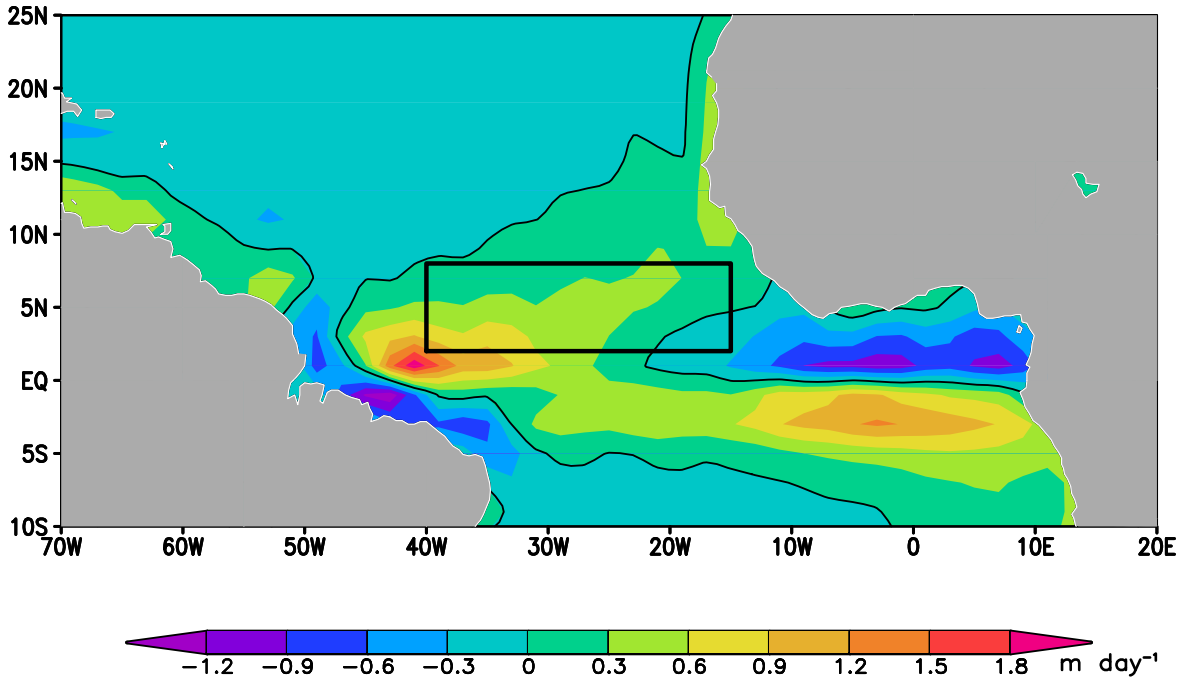

Fig. S1 Climatological MAM wind-driven upwelling (positive upward) during 1982–2010. The zero contour is shown as a black line. Black box encloses the equatorial North Atlantic region.

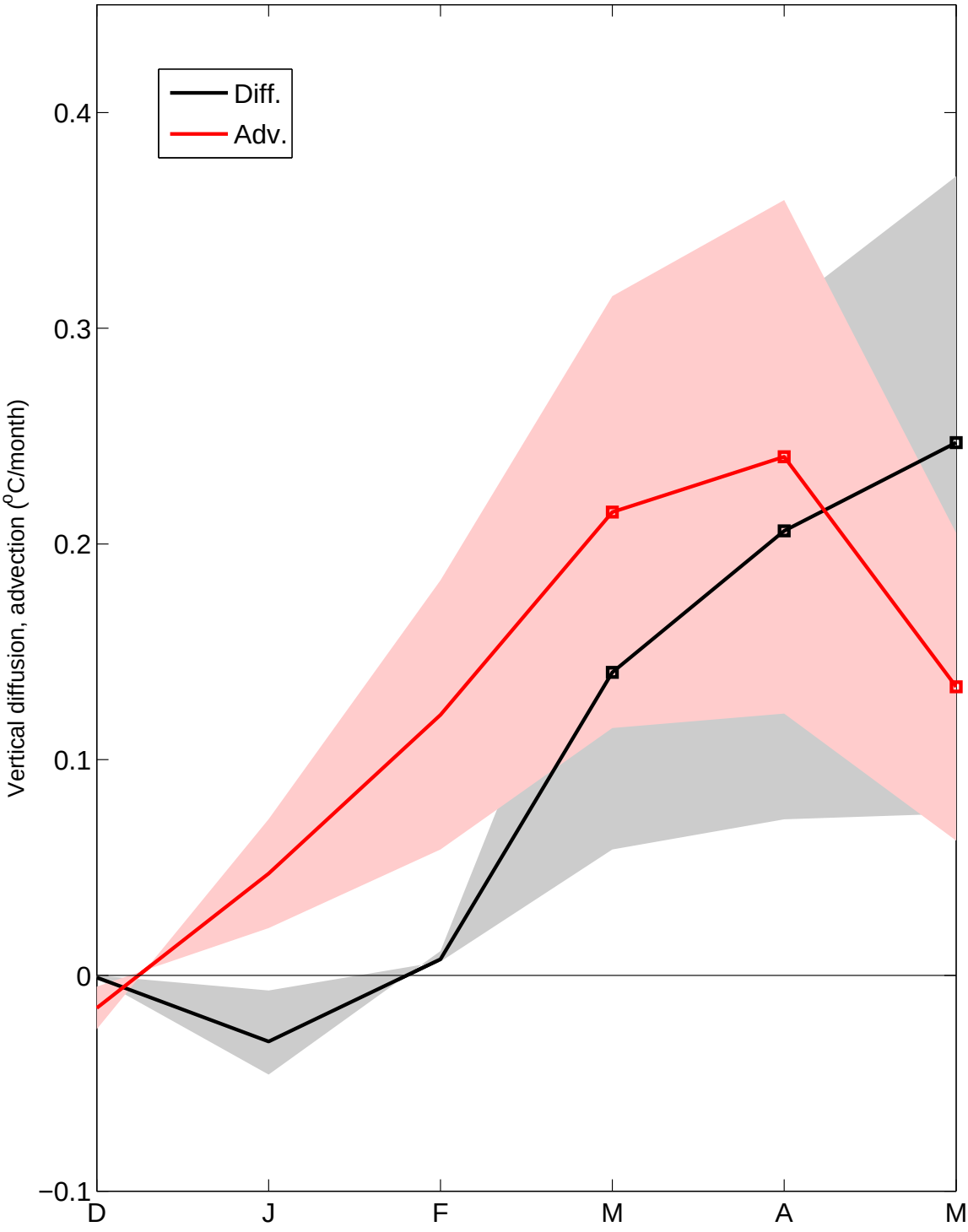

Fig. S2 Vertical turbulent diffusion (black) and advection (red) anomalies averaged in the ENA (2°N–8°N, 15°W–40°W) and regressed onto the first EOF of MAM SST (shown in Fig. 1). Squares indicate values that are significant at the 95% level. Shading represents error bars.

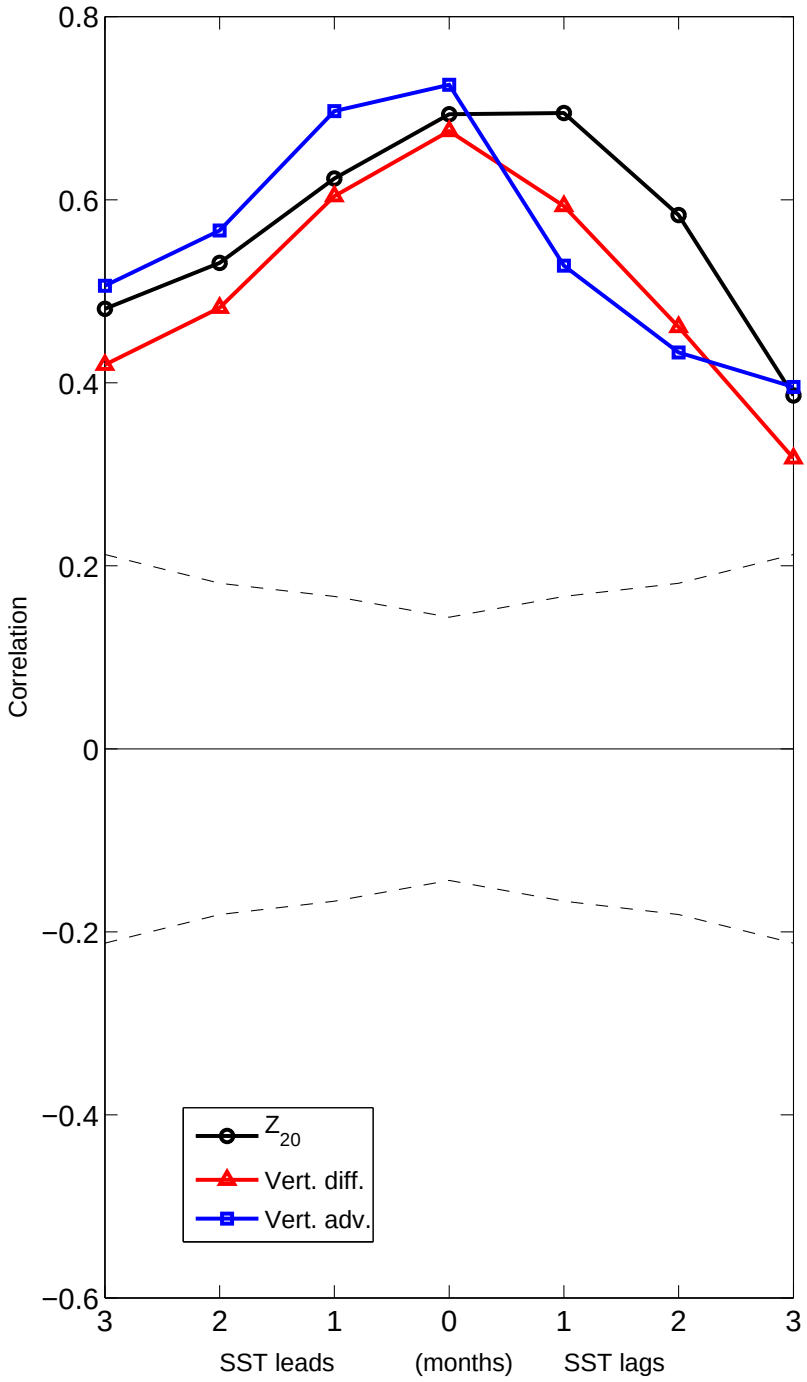

Fig. S3 Lagged correlations of thermocline depth (solid black), vertical turbulent diffusion (red), and vertical advection (blue), averaged in the ENA region (2°N–8°N, 15°W–40°W), with the cross-equatorial gradient of SST, defined as SST in the ENA minus SST averaged between 0°–8°S, 0°–30°W. Correlations are performed for 1982–2010 during Jan–Jun. Dashed lines are the 95% significance level.

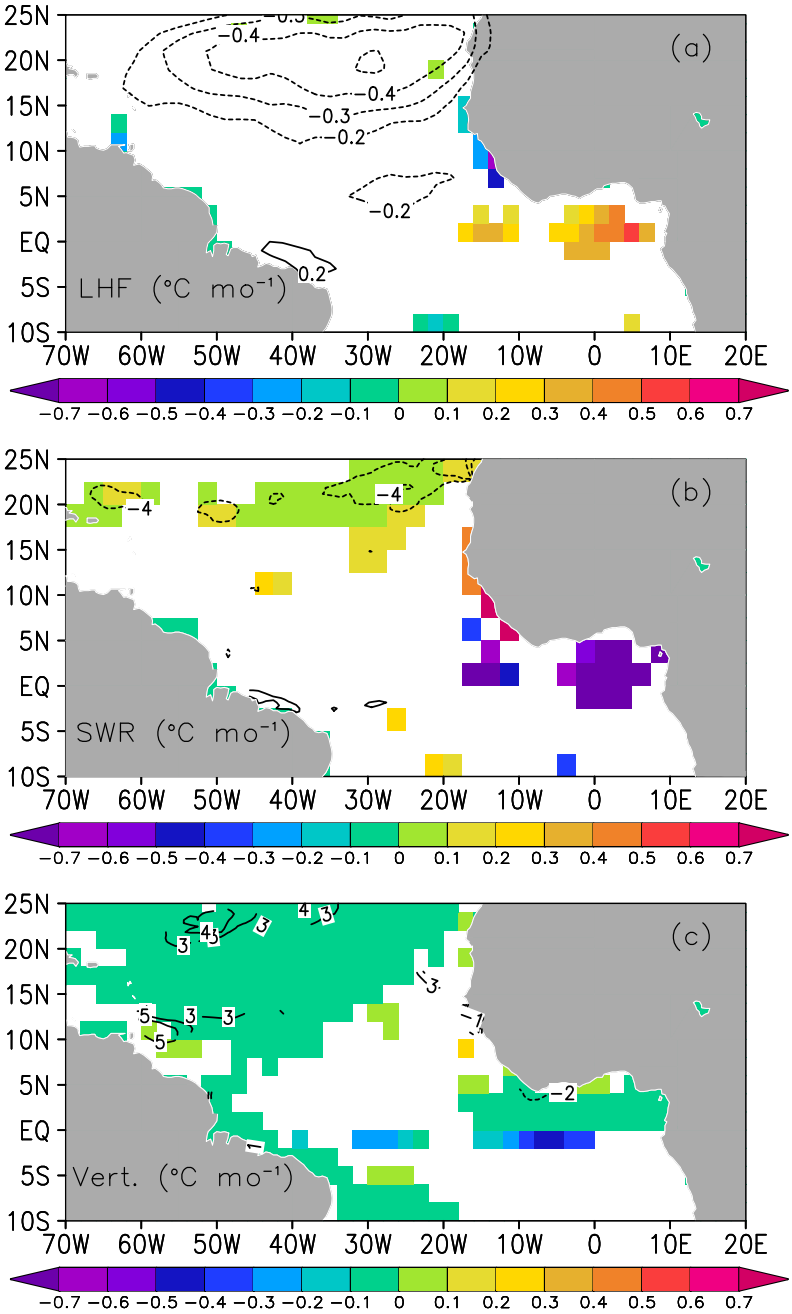

Fig. S4 (a) DJF wind speed (contours, m s^{-1}) and latent heat flux (shaded, °C mo^{-1}, positive indicates warming of the ocean) anomalies regressed onto the first EOF of MAM SST. Values are shown only where significant at the 95% level. (b) Same as (a) except anomalies of mixed layer depth (contours, m) and surface shortwave radiation (shading, °C mo^{-1}). (c) Same as (a) except contours are thermocline depth (estimated as the depth of the 20°C isotherm, in meters) and shading is vertical heat flux at the base of the mixed layer (°C mo^{-1}).

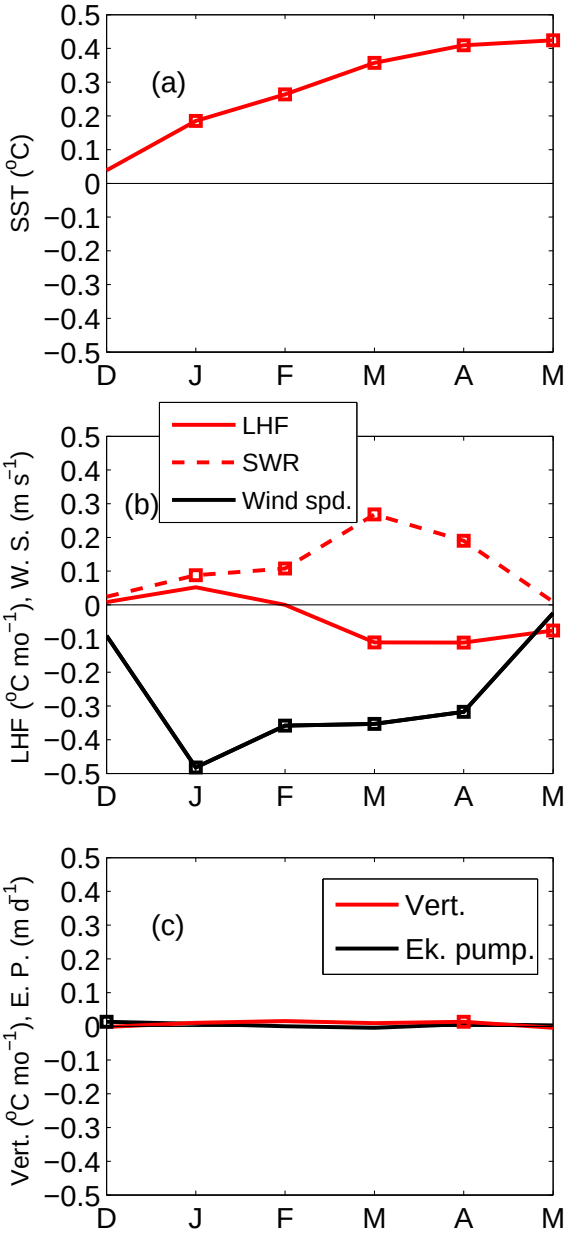

Fig. S5 (a) SST averaged in the tropical North Atlantic (8°N–20°N, 20°W–45°W) and regressed onto the first EOF of MAM SST during Dec–May 1982–2010. Squares indicate regression coefficients that are significant at the 95% level. (b) Same as (a) except for latent heat flux (solid red), surface shortwave radiation (dashed red), and surface wind speed (black). (c) Same as (a) except for vertical heat flux at the base of the mixed layer (red) and wind-driven upwelling (black curve, with positive values indicating downward velocity). Positive values of LHF, SWR, and vertical heat flux (red curves in (b) and (c)) indicate warming of the mixed layer.

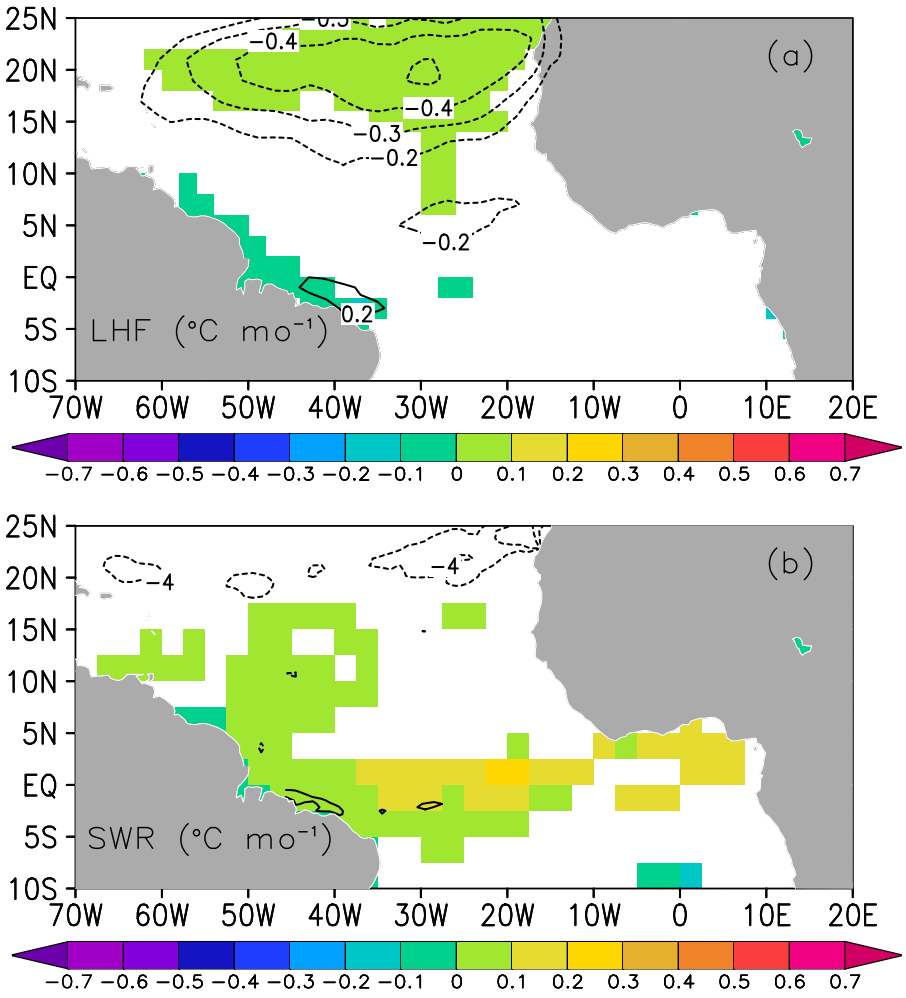

Fig. S6 (a) DJF wind speed (contours, m s^{-1}) and latent heat flux (shaded, °C mo^{-1}, positive indicates warming of the ocean) anomalies regressed onto the first EOF of MAM SST. Values are shown only where significant at the 95% level. (b) Same as (a) except anomalies of mixed layer depth (contours, m) and surface shortwave radiation (shading, °C mo^{-1}). Climatological MLD was used for the calculation of LHF and SWR in (a) and (b).

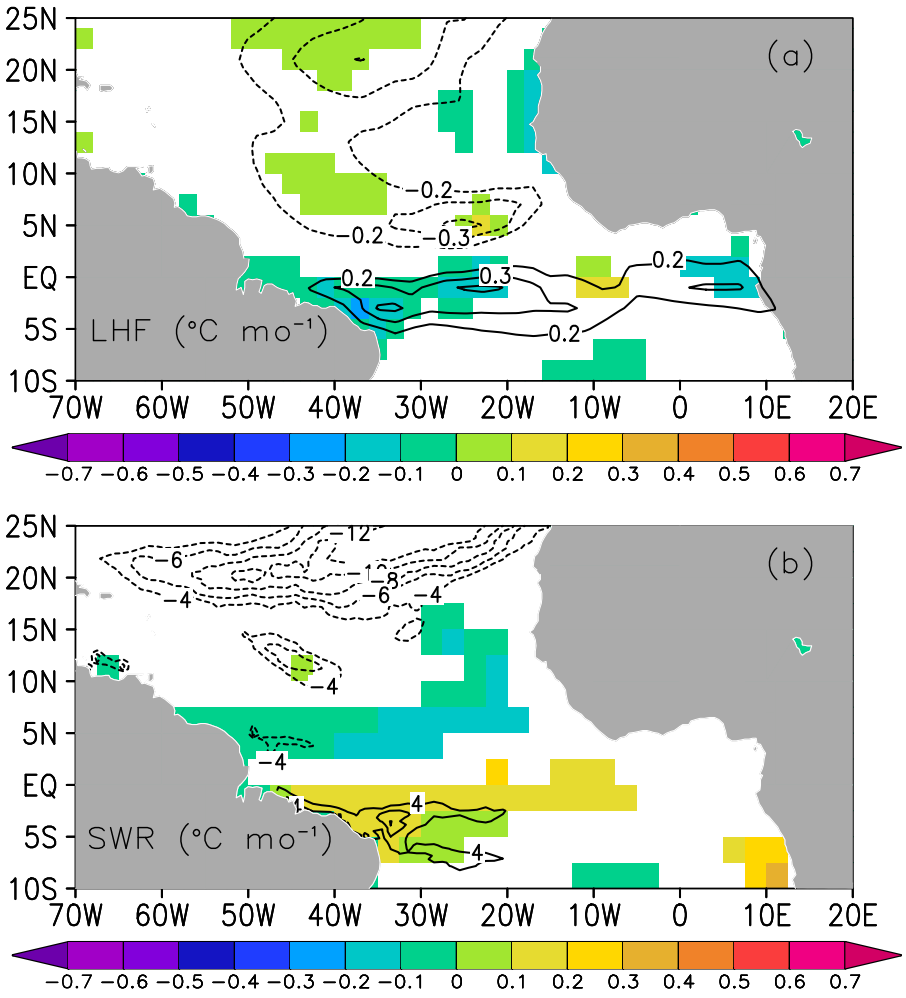

Fig. S7 (a) MAM wind speed (contours, m s^{-1}) and latent heat flux (shaded, °C mo^{-1}, positive indicates warming of the ocean) anomalies regressed onto the first EOF of MAM SST. Values are shown only where significant at the 95% level. (b) Same as (a) except anomalies of mixed layer depth (contours, m) and surface shortwave radiation (shading, °C mo^{-1}). Climatological MLD was used for the calculation of LHF and SWR in (a) and (b).

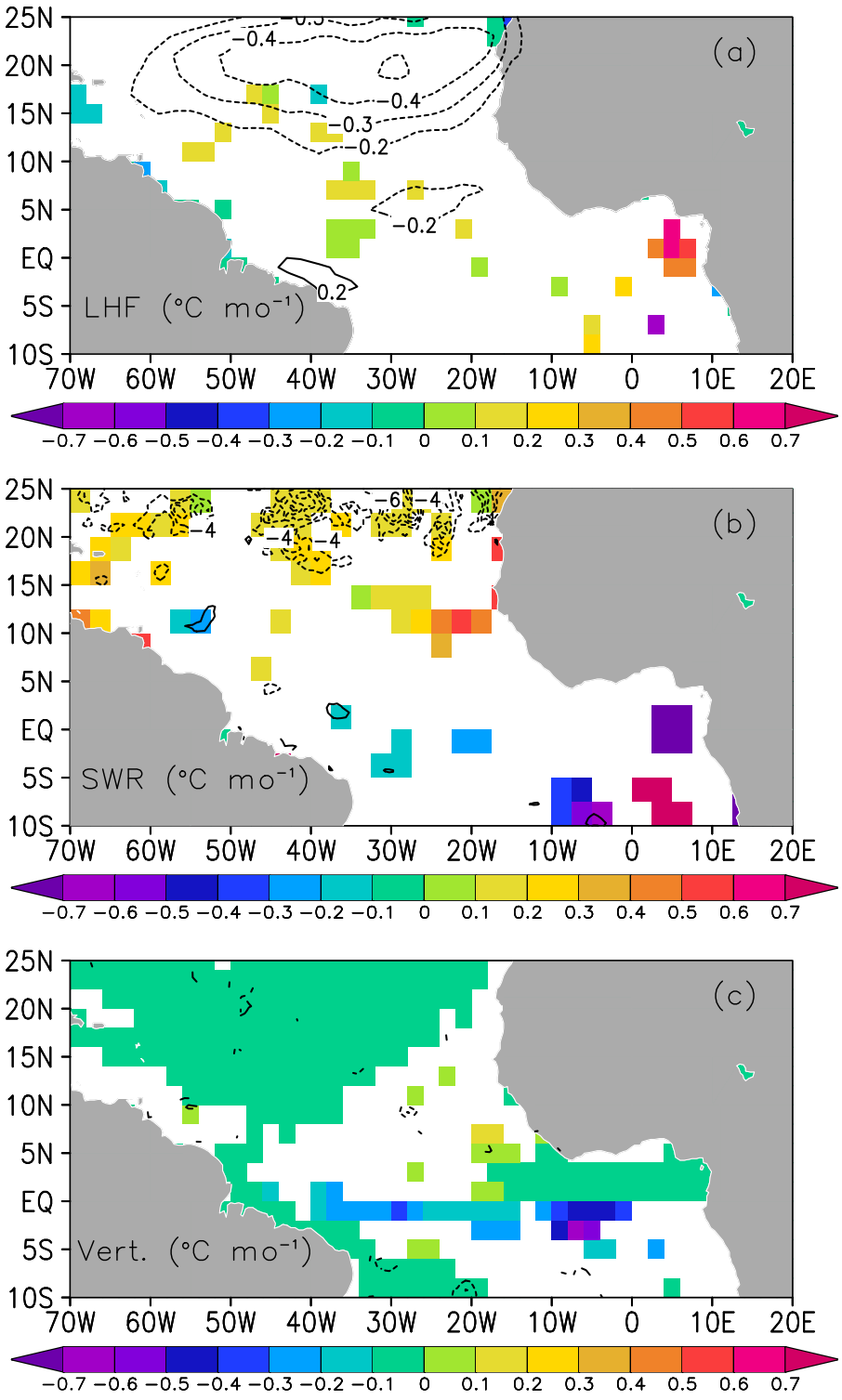

Fig. S8 Same as Fig. S4 except latent heat flux (a), shortwave radiation and mixed layer depth (b), and vertical advection and thermoclined depth (c) were calculated from SODA instead of GODAS.

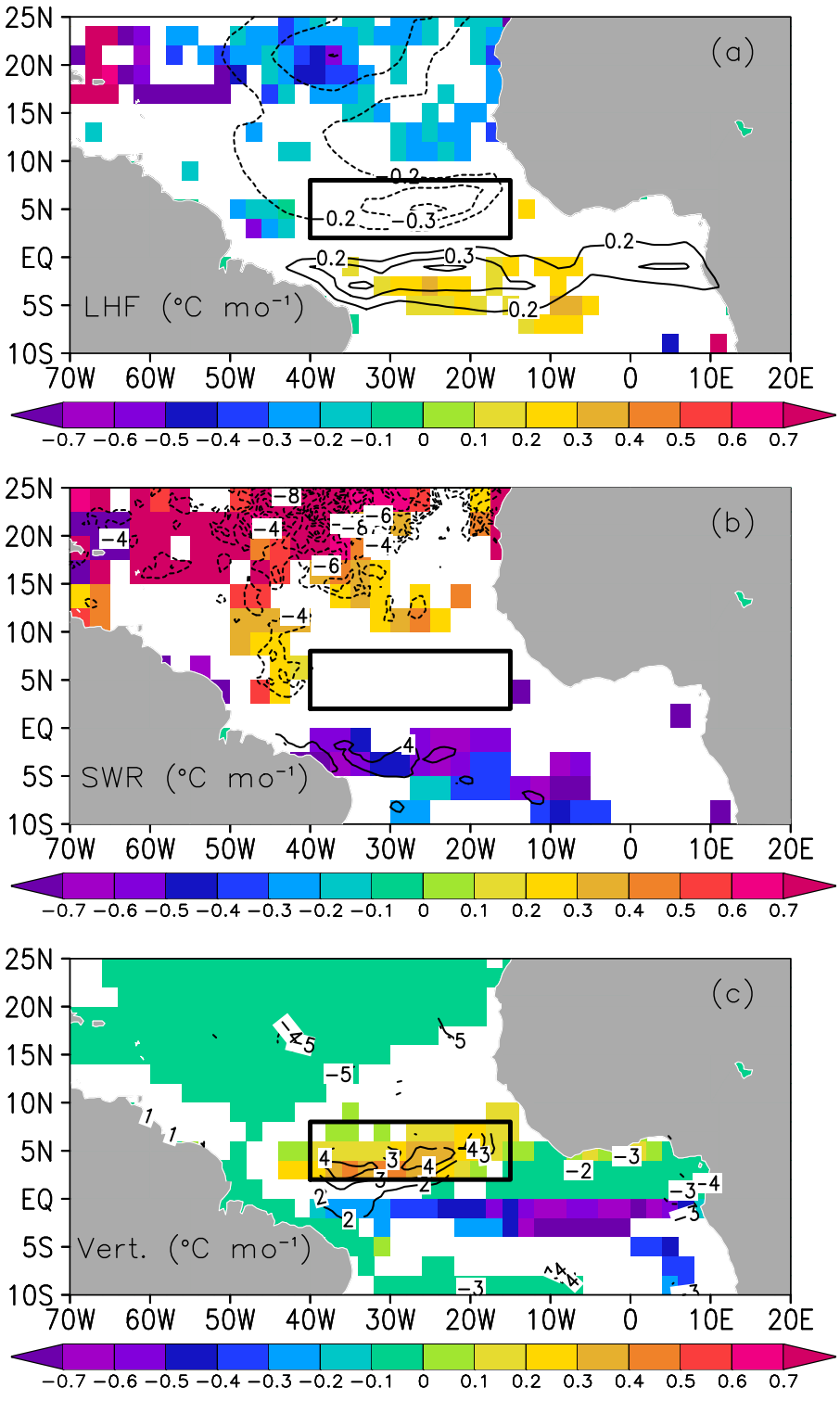

Fig. S9 Same as Fig. S8 except MAM anomalies regressed onto first EOF of MAM SST. Black boxes enclose the equatorial North Atlantic region.